

Definition of Tomographic SAR Configurations for Forest Structure Applications at L-band

Victor Cazcarra-Bes, Matteo Pardini, *Member, IEEE*, Konstantinos Papathanassiou, *Fellow, IEEE*

Abstract—Synthetic Aperture Radar Tomography (TomoSAR) at lower frequencies allows the reconstruction of the 3-D radar reflectivity of volume scatterers allowing access to their physical 3-D structure by means of multi-angular SAR acquisitions. The performance of the reconstruction critically depends on the number and (spatial) distribution of the tomographic acquisitions (tracks). This dependency is addressed in this letter with respect to forest applications (volume scatters) at L-band. The letter discusses the optimum definition of tomographic configurations based on the peak sidelobe level (PSL) of the point spread function (PSF). For demonstration, a tomographic data set consisting of fifteen acquisitions acquired by the DLR's F-SAR system at L-band over the Traunstein test site in Germany is used, complemented by airborne lidar measurements. Three different reconstruction algorithms (Fourier beamforming, Capon beamforming, and compressive sensing) are implemented and compared to each other for scenarios with a reduced number of acquisitions. Although the limitation of the specific forest, the results show the potential of using the PSL of the PSF to define tomographic configurations optimised for forest structure applications.

Index Terms—Forest Structure, Synthetic Aperture Radar Tomography, L-band, Baseline Configuration, Spatial Distribution of Acquisitions

I. INTRODUCTION

SYNTHETIC Aperture Radar (SAR) tomography (TomoSAR) allows the reconstruction of the 3-D radar reflectivity of volume scatterers by combining multiple SAR images acquired with slightly different incidence (or look) angles along spatially displaced tracks (or orbits) [1]. At lower frequencies (L- or P-band) the reconstructed 3-D radar reflectivity allows to characterise the 3-D forest structure [2], [3]. This potential to provide forest physical structure information, at the high spatial and temporal resolution(s) typical of SAR systems, makes TomoSAR a key element of future spaceborne SAR missions aiming forest applications, e. g. ESA's BIOMASS and DLR's Tandem-L.

In the absence of unique solutions of the general TomoSAR reconstruction problem, different algorithms (model-based, model-free or hybrid ones) have been proposed and used in the literature [4], [5]. The most popular ones are the Fourier beamforming (FB) [6], the Capon beamforming (CB) [6] (model-free algorithms) and compressive sensing (CS) [7], [8], [9] (hybrid algorithms) relying on sparsity bases. For volume scatterers, each algorithm has its strengths and weaknesses depending on the application requirements and system limitations.

Besides the choice of the algorithm, the reconstruction performance for forest structure applications critically depends on the number and the spatial distribution of the tracks

(or orbits) of the tomographic acquisitions. This is because they define three important reconstruction parameters: 1) the vertical resolution, which is associated with the ability to resolve individual forest layers, 2) the Height of Ambiguity (HoA) that defines the unambiguous reconstruction height interval and 3) the Peak Sidelobe Level (PSL) that expresses the signal ratio between the first sidelobe and the main lobe of the Point Spread Function (PSF).

Each image pair y_m, y_n with $m, n = 1, \dots, M$ of a TomoSAR data set consisting of M SAR images, is characterised by the so-called vertical wavenumber k_z , that expresses the sensitivity (i.e. the derivative) of the phase (of the complex conjugate product of two Single Look Complex (SLC) images) to a height change [1]:

$$k_z(m, n) = \frac{4 \pi \Delta \theta (m, n)}{\lambda \sin(\theta)}, \quad (1)$$

where $\Delta \theta (m, n)$ is the incidence angle difference associated with the pair formed by the m th and the n th acquisitions, λ is the wavelength, and θ is the incidence angle. The vertical resolution and the HoA are defined as:

$$\delta_z = \frac{2\pi}{k_{z \max}}, \quad z_{\text{amb}} = \frac{2\pi}{k_{z \min}} \quad (2)$$

where $k_{z \min} = \min_{m,n} \{k_z(m, n)\}$ and $k_{z \max} = \max_{m,n} \{k_z(m, n)\}$. $k_{z \max}$ and $k_{z \min}$ are directly proportional to the maximum and minimum track displacements, respectively.

The PSF, for a large number and uniformly displaced acquisitions becomes a sinc² function, and therefore the PSL is equal to -13.26 dB. For a low number of acquisitions, the PSL becomes:

$$^1PSL \simeq 10 \log_{10} \left(\frac{\sin^2(1.4311\pi)}{M^2 \sin^2\left(\frac{1.4311\pi}{M}\right)} \right). \quad (3)$$

However, the expression in (3) holds only for a uniform distribution of acquisitions. If the distribution of k_z becomes non-uniform, the PSL will change. The optimization of the PSF for sparse and irregular arrays has been extensively addressed in the literature [6], [10]. This letter addresses the case of forest scatterers, i.e. vertically extended volume scatters, for a particular TomoSAR application. In [11], the optimization of uniformly distributed tomographic configurations has been

¹Note that in (3) the position of the first side lobe has been approximated to be always in the same position, which is not strictly true as its position slightly changes with M .

discussed using MUSIC, a model based algorithm, which pre-defines the number of phase centers before the TomoSAR inversion. The tomographic focusing of point-like scatterers for irregular distributed tomographic configurations has been addressed in [12]. For forest applications, in [13] the problem of increased sidelobes arising from non-uniform distributions has been treated, but without attempting any optimization or comparison with external data (Lidar).

In this letter, a more complete treatment is attempted by selecting non-uniform acquisitions (in terms of position of the tracks) based on the PSL of the PSF and realistic reconstruction requirements (in terms of vertical resolution and HoA) for forest structure applications. The selection of the tracks (from all possible combinations) is carried out by an iterative minimization process based on the PSL. The requirements for the PSL have been derived by analysing a reference data set of 15 uniformly displaced acquisitions over a temperate forest in Germany. For the tomographic reconstruction, the results obtained by using three algorithms (FB and CB and CS) are compared and discussed together with high-resolution lidar data.

II. TEST SITE AND TOMOGRAPHIC DATA SET

The test site is a temperate forest located in Traunstein, Germany, comprising different forest structure types. In May 2017, a fully polarimetric L-band tomographic repeat-pass data set has been acquired by the DLR's F-SAR airborne sensor consisting of fifteen uniformly distributed acquisitions with a horizontal distance of about 5 m between them. This results in a uniformly distributed set of vertical wavenumbers (k_z), from 0 rad/m to 1.05 rad/m, associated to a vertical Rayleigh resolution of 6 m and a HoA of about 85 m. The spatial resolutions of the SLC images are 1.28 m and 0.6 m in slant-range and azimuth respectively. This full data set will be used in the following as the reference scenario.

For comparison, airborne Lidar data also acquired in 2016 are used. Figure 1 shows the Lidar derived forest top height map of the site that visualizes the heterogeneity in the site. The forest can be divided in polygons assuming the same forest structure type inside each of them: The west part (left) is composed by multi-layer forest stands (indicated by the black polygon), in the middle there is a gap with a few scattered trees (red polygon), and towards the east (right) there are mainly mono-layer homogeneous stands (orange and blue polygons).

III. REFERENCE DATA SET

After SAR processing, the fifteen SLC SAR images (coregistered and phase calibrated with respect to each other) are ready to be used for tomographic processing [1]. The M tomographic images are arranged in form of a (data) vector $\mathbf{y} = [y_1, \dots, y_M]^T$, where $(\cdot)^T$ denotes the transpose operator, and it is used to form the covariance matrix $\mathbf{R} = E\{\mathbf{y}\mathbf{y}^H\}$, where $(\cdot)^H$ indicates the Hermitian operator and $E\{\cdot\}$ is the statistical expectation approximated by the mean value of neighboring samples. The FB, CB and CS (implemented by means of a Symmlet wavelet with four vanishing moments and two levels of decomposition) are applied on the covariance

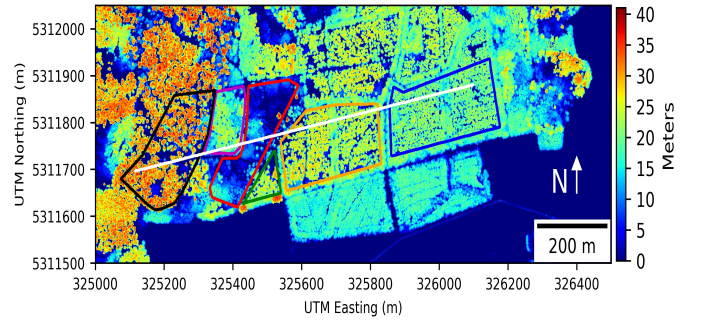


Fig. 1: Lidar height over the Traunstein forest. Each polygon represents a homogeneous forest structure type.

matrix \mathbf{R} using the associated vertical wavenumber k_z . A detailed description of the CS algorithm and the specific parameters used in this letter, as well as a comparison with FB and CB can be found in [9].

A. Forest Structure from Profiles: Lidar and Radar

Figure 2 shows the tomographic profiles across the transect indicated by the white line in Figure 1 for FB (a), CB (b) and CS (c). Also, in (d) the Lidar profiles over the same area are shown. The quality of the reconstructions is confirmed by the PSF shown in Figure 3(a), as it is characterised by sidelobes below -13 dB (with respect to the main lobe). FB and CB show very similar results with a slightly better resolution for CB, as confirmed by the narrower reflectivity layers. The CS results are more sparse, characterized by a higher vertical resolution, but also with some erroneously reconstructed maxima in the reflectivity profiles compared to FB and CB [9].

In order to evaluate better the achieved performance, Figure 4(a) shows the mean profiles over the polygons highlighted in Figure 1. There is a consistent qualitative agreement between the Lidar profile (black line) and the tomographic reconstructions, in terms of the number and position of the canopy layers, reflecting the different forest structure of each area. There are some differences between the algorithms, as for example the better discrimination of the maxima in the CS profile (blue line). But, in general, the three reconstructions are similar, indicating the same underlying structure. Therefore, it can be concluded that, for the reference data set, the different forest structure types can be distinguished and the choice of the reconstruction algorithm is not crucial under these very favourable conditions.

B. Requirements for Forest Structure Applications

While the requirements on vertical resolution (on the order of 5-15 m) and HoA (higher than the tallest trees in the scene) are well understood, the impact of the sidelobe levels is not. Sidelobes of strong scatterers can be confused with mainlobe maximas of weaker scattering contributions. For example, sidelobes of the ground scattering component may be misinterpreted as real canopy layers. Accordingly, a requirement in terms of the power difference between the main lobe and the maximum sidelobe (i.e the PSL) is required. In

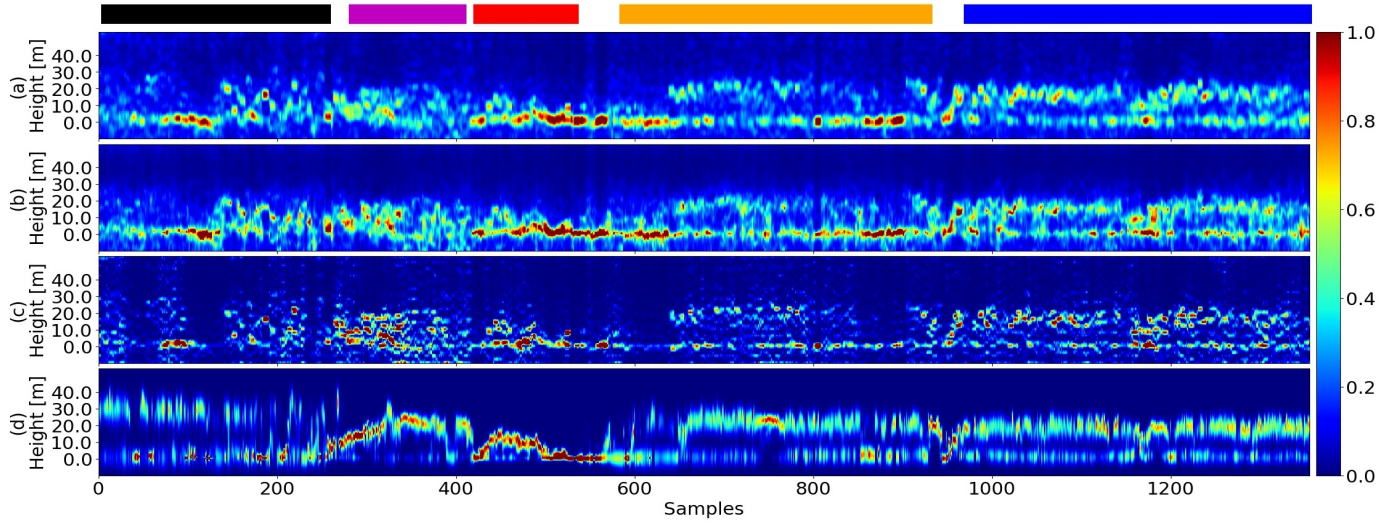


Fig. 2: (a) Fourier Beamforming, (b) Capon Beamforming, (c) Compressive Sensing tomographic results for the HV channel and (d) Lidar profiles over the white line from Figure 1. Each figure is normalized by its own maximum. One sample represents a spacing of 0.8 meters. The colored rectangles on the upper part refer to the areas defined in Figure 1.

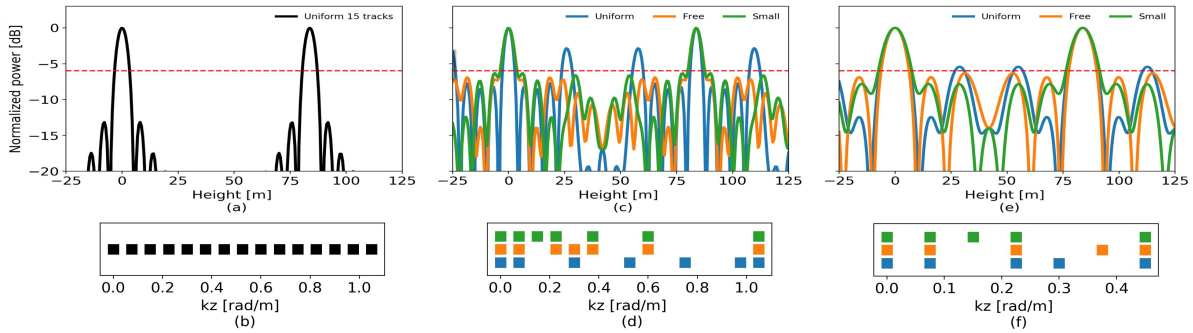


Fig. 3: (a) Point Spread Function (PSF) and (b) k_z distribution for fifteen acquisitions; (c) PSF and (d) k_z distributions for seven acquisitions; (e) PSF and (f) k_z distributions for five acquisitions. The PSF's in (a), (b) and (c) are obtained using the Fourier beamforming.

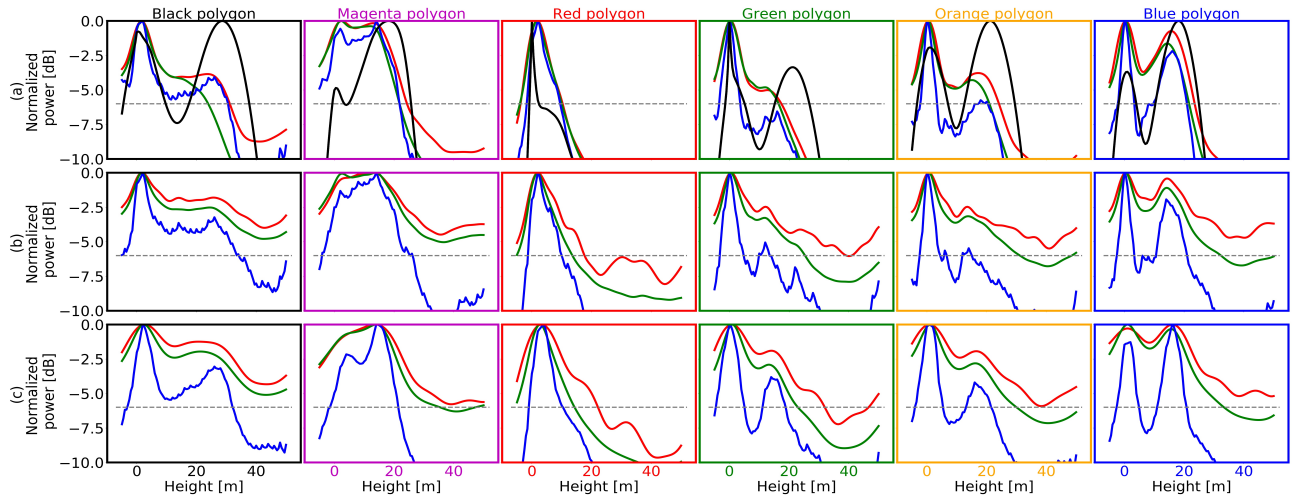


Fig. 4: Mean profiles over the polygons (each column represents one) defined in Figure 1 for lidar point cloud (black) and the tomographic SAR algorithms: Fourier beamforming (red), Capon beamforming (green) and compressive sensing (blue) for the HV channel. Each row represents a different distribution of acquisitions: (a) Fifteen uniform distributed acquisitions (see Figure 3(b)), (b) *small* distribution scenario with seven acquisitions (see green colour Figure 3(d)) and (c) *small* distribution scenario with five acquisitions (see green colour Figure 3(f)). The grey dashed line indicates the threshold of -6 dB.

the context of forest structure applications, where the local maxima of the reconstructed reflectivity are interpreted as canopy layers [2], [3], the power of the sidelobes should be lower than the reflectivity maxima corresponding to the canopy layers.

In order to derive such a requirement, the difference of the powers of the two main reflectivity maxima is evaluated as obtained by the three algorithms (FB, CB and CS) in the different polarizations (HH, HV and VV) for the reference tomographic data set. The obtained power differences for each of the polygons (i.e. structure types) of Figure 1 are shown in Table I. Except for the red polygon, where only one scattering contribution (i.e. the ground) dominates, all other differences lie between 2 and 5 dB. Accordingly, a 6 dB difference, between the maxima and the highest sidelobe, appears sufficient to separate the canopy layers in the different forest structure areas. Note that, the ratios for CB, FB and CS are similar. This implies that the posed requirement in terms of PSL (-6 dB) is independent of the selection of the algorithm and it can be therefore analyzed through the PSF.

TABLE I: Power difference in dB between the two main canopy layers.

Algorithm,Channel	Blue polygon	Orange polygon	Green polygon	Magenta polygon	Black polygon
FB,HH	-2.84 (± 1.37)	-3.67 (± 1.31)	-5.09 (± 1.25)	-2.92 (± 1.37)	-3.1 (± 1.43)
FB,HV	-1.87 (± 1.02)	-2.52 (± 1.25)	-3.47 (± 1.37)	-2.22 (± 1.31)	-2.37 (± 1.31)
FB,VV	-2.37 (± 1.19)	-3.28 (± 1.25)	-4.2 (± 1.31)	-2.44 (± 1.31)	-2.68 (± 1.37)
FB,HH+HV+VV	-2.01 (± 1.08)	-3.1 (± 1.25)	-4.32 (± 1.31)	-2.44 (± 1.37)	-2.68 (± 1.37)
CB,HH	-2.92 (± 1.25)	-3.87 (± 1.31)	-5.09 (± 1.31)	-2.6 (± 1.43)	-3.47 (± 1.43)
CB,HV	-1.8 (± 1.02)	-2.76 (± 1.31)	-3.37 (± 1.49)	-2.08 (± 1.31)	-2.06 (± 1.37)
CB,VV	-2.52 (± 1.19)	-3.57 (± 1.31)	-4.32 (± 1.43)	-2.29 (± 1.31)	-3.01 (± 1.43)
CB,HH+HV+VV	-2.15 (± 1.08)	-3.47 (± 1.25)	-4.44 (± 1.31)	-2.15 (± 1.37)	-3.1 (± 1.37)
CS,HH	-2.92 (± 1.37)	-3.57 (± 1.49)	-4.69 (± 1.49)	-2.68 (± 1.37)	-2.76 (± 1.49)
CS,HV	-1.87 (± 1.14)	-2.44 (± 1.37)	-3.19 (± 1.49)	-1.94 (± 1.19)	-2.15 (± 1.31)
CS,VV	-2.44 (± 1.25)	-3.1 (± 1.43)	-3.77 (± 1.49)	-2.22 (± 1.25)	-2.37 (± 1.37)
CS,HH+HV+VV	-2.76 (± 1.31)	-3.57 (± 1.43)	-4.56 (± 1.43)	-2.44 (± 1.31)	-2.68 (± 1.43)

The first number represents the mean value (in the polygon) of the power difference (in dB) between the two highest local maxima of the tomographic result. The number in brackets corresponds to the standard deviation. For the tomographic processing the fifteen available acquisitions have been used.

IV. SCENARIOS WITH A REDUCED NUMBER OF ACQUISITIONS

Having established the requirements on the reconstructed reflectivity in terms of the HoA ($>50\text{m}$) and PSL (-6 dB), downscaled tomographic configurations still able to fulfil these requirements are investigated. For the requirement of the vertical resolution, two scenarios are evaluated: One with the maximum possible vertical resolution (6 m) and one changing the vertical resolution (from 21 m to 6 m). For both scenarios, three vertical wavenumber distributions are discussed: 1) *Uniform* wavenumber distribution with equidistant acquisitions. 2) *Small* wavenumber distribution, i.e. distributions with three small vertical wavenumbers (up to 0.22 rad/m) that can be used for forest height estimation in addition to TomoSAR. 3) *Free* wavenumber distribution, where no restriction on the distribution apply.

For each of the mentioned scenarios, the optimization selects (from all possible configurations) the configuration of tracks that provides the lowest possible PSL. Note here,

that the definition of possible configurations is constrained by the fifteen vertical wavenumbers k_z of the experimental data set described in Section II, and by the requirements on the HoA and vertical resolution. In addition, the formation of the uniform distribution requires the availability of equidistant tracks at a given distance, which is not always possible to be formed out from the available k_z in the data set. The minimum possible track separation corresponds to a HoA of 84 m. The next smaller possible separation corresponds to a HoA of only 42 m, which is almost the height of the tallest trees in the scene. To avoid any misinterpretation, the HoA is fixed to 84 m. The maximum possible acquisition separation available corresponds to a vertical (Rayleigh) resolution of 6 m. In the following, scenarios with a reduced number of tracks resulting in a deformed PSF and/or a reduced vertical resolution are investigated by thinning the reference data set. Therefore, for each of the scenarios in Section IV-A and IV-B, an iterative minimization procedure is carried out in order to find the distribution of tracks that provides the lowest possible PSL fulfilling the corresponding requirements.

A. Maximum Possible Vertical Resolution

Table II shows the PSL level (in dB) for the three distributions, with an increasing number of acquisitions and keeping constant the vertical resolution to 6 m (i.e. the same maximum track separation). One can see that, in order to fulfil the sidelobe requirement for the *free* and *small* wavenumber distribution, at least seven acquisitions are required. In the case of the *uniform* distribution, an increase to eleven acquisitions is needed to have a sidelobe lower than -6 dB.

TABLE II: Peak sidelobe level (in dB) of the PSF obtained with FB for the different distributions with a vertical resolution of 6 m.

# Acquisitions	3	4	5	6	7	8	9	10	11	12	13	14	15
Uniform ¹	-0.2	-0.5	-1.2	-1.7	-2.8	-5.2	-5.1	-4.4	-7.6	-7.5	-8.3	-10.2	-13.13
Free	-0.2	-2	-4.4	-5.5	-6.9	-8.5	-9.8	-10.8	-11.3	-12.9	-13.4	-14.23	-13.13
Small	-	-	-1.1	-4.2	-6.3	-8.5	-9.7	-10	-11.3	-12.9	-13.4	-14.23	-13.13

¹The uniform distributions are not always completely uniform as the k_z values are limited to the original positions and two fixed positions are needed to fulfil the requirements on the HoA and vertical resolution.

Figure 3(c) and (d) show the PSF for the case of seven acquisitions and the associated k_z values for each distribution. As already indicated, the *uniform* wavenumber distribution does not fulfil the -6 dB sidelobe requirement with seven acquisitions. However, compared to the other distributions, the main lobe is narrower and has a larger distance to the sidelobe. In the case of *free* and *small* wavenumber distributions, a wider main lobe and a reduced sidelobe distance goes in favour of lower sidelobe levels, that in both cases fulfil the -6 dB requirement. The difference between the *free* and the *small* wavenumber distribution is not significant, with an irregular PSF and similar levels for the PSL. The fact that the *small* distribution is of advantage for forest height estimation makes it, in our view, the preferred one.

Figure 4(b) compares the profiles obtained in the case of the *small* wavenumber configuration for seven acquisitions and a vertical resolution of 6 m. The main difference to

the fifteen acquisitions scenario (Figure 4(a)) is the increased sidelobe level. Especially affected is the FB reconstruction (in red) where the identification of main scattering contributions from local maxima becomes more difficult. Anyhow, the reflectivity profile appears correct (compared to the Lidar) for all polygons, except for the green one. A possible explanation for this polygon is the small amount of samples available to characterize this area. The advantage of a high vertical resolution is reflected in the magenta polygon, where the two main local maxima are separated in the CB and CS reconstructions, but not in the FB. For FB, the increase of the sidelobe levels mix the two maxima, making impossible to distinguish the two layers.

B. Tomographic Scenario with Five Acquisitions

A space borne tomographic data set may consist of four to five acquisitions. From Table II follows that five acquisitions do not allow sidelobe levels below -6 dB keeping the vertical resolution at 6 m. A better PSL performance can only be achieved at the cost of vertical resolution (i.e. by reducing the maximum track separation). Table III shows the PSL values depending on the vertical resolution for the three wavenumber distributions associated to five acquisitions. In order to fulfil the -6 dB PSL requirement, the vertical resolution has to be reduced to 14 m for the *free* and *small* distributions and to 16.7 m for the *uniform* one.

TABLE III: Peak sidelobe level (in dB) of the PSF obtained with FB for the different distributions with five acquisitions.

Vertical Res. ¹	21	16.7	14	12	10.5	9.3	8.4	7.6	7	6.4	6
Uniform ²	-12	-8.3	-5.4	-4.4	-3	-5.5	-2	-4.2	-2.8	-1.2	-1.2
Free	-12	-6.9	-6.3	-5.2	-5.3	-5.4	-4.5	-4.7	-5.16	-4.7	-4.4
Small	-12	-8.3	-7.8	-5.3	-3.8	-2.9	-2.3	-1.8	-1.5	-1.2	-1.1

¹Rayleigh resolution in meters. ²The uniform distributions are not always completely uniform as the k_z values are limited to the original positions and two fixed positions are needed to fulfil the requirements on the HoA and vertical resolution.

Figure 3(e) and (f) show the PSF for a vertical resolution of 14 m using five acquisitions and the corresponding vertical wavenumbers. The lower resolution is reflected on a wider main lobe respect to the one obtained in Figure 3(c). The loss of resolution goes in favour of a reduction of the PSL. The performance across the three distributions is now more similar, with slightly higher values of the PSL in the *uniform* distribution. Also here, the *small* distribution case appears the favoured one. Figure 4(c) shows the profiles obtained by the three algorithms for the *small* distribution. In contrast to the results in Figure 4(b), the profiles appear cleaner allowing a better localization of local maxima. However, the loss in vertical resolution compare to the scenarios with seven and fifteen acquisitions is evident. Nevertheless, for this specific data set, only the magenta polygon appears to be affected by the degraded resolution. In that polygon, while CS is able to detect the two layers, FB and CB fail mixing both maxima. Regarding the difference between the algorithms, FB shows again the lower contrast between the maxima as well as with the sidelobes. However, CS shows a higher contrast that allows a better discrimination of the maxima.

V. CONCLUSIONS

This letter analyzes the impact of the number and distribution of acquisitions in SAR tomography for forest structure applications. Starting from a data set with fifteen acquisitions, different wavenumber distributions with a reduced number of acquisitions have been optimized from all available combinations, with respect to the peak sidelobe level and requirements such as fixed values of some wavenumbers. Constraining the wavenumber distribution to achieve the maximum possible vertical resolution of 6 m, the obtained results indicate that a minimum number of seven acquisitions is necessary to suppress the sidelobes below -6 dB. For a tomographic scenario with only five acquisitions, a sidelobe suppression better than -6 dB can be achieved only by reducing the vertical resolution down to 14 m. For both scenarios, the results have been discussed by means of three different TomoSAR reconstruction algorithms (Fourier beamforming, Capon beamforming and compressive sensing), indicating the effect of the choice of the reconstruction algorithm. The reduction of vertical resolution (in the actual case from 6 to 14 m) may be problematic for areas with multiple canopy layers, as it compromises the discrimination of different forest structure types. In this sense, a possible compromise could be to use 6 acquisitions to increase the vertical resolution to 10.5 m and, at the same time, keep the PSL below -6 dB for all distributions.

REFERENCES

- [1] A. Reigber and A. Moreira, "First demonstration of airborne sar tomography using multibaseline l-band data," *IEEE Transactions on Geoscience and Remote Sensing*, vol. 38, no. 5, pp. 2142–2152, 2000.
- [2] M. Tello, V. Cazcarra-Bes, M. Pardini, and K. Papathanassiou, "Forest structure characterization from sar tomography at l-band," *IEEE Journal of Selected Topics in Applied Earth Observations and Remote Sensing*, no. 99, pp. 1–13, 2018.
- [3] V. Cazcarra-Bes, M. Tello-Alonso, R. Fischer, M. Heym, and K. Papathanassiou, "Monitoring of forest structure dynamics by means of l-band sar tomography," *Remote Sensing*, vol. 9, no. 12, p. 1229, 2017.
- [4] S. Tebaldini, "Single and multipolarimetric sar tomography of forested areas: A parametric approach," *IEEE Transactions on Geoscience and Remote Sensing*, vol. 48, no. 5, pp. 2375–2387, 2010.
- [5] O. Frey and E. Meier, "Analyzing tomographic sar data of a forest with respect to frequency, polarization, and focusing technique," *IEEE Transactions on Geoscience and Remote Sensing*, vol. 49, no. 10, pp. 3648–3659, 2011.
- [6] P. Stoica, R. L. Moses, *et al.*, "Spectral analysis of signals," 2005.
- [7] E. Aguilera, M. Nannini, and A. Reigber, "A data-adaptive compressed sensing approach to polarimetric sar tomography of forested areas," *IEEE Geoscience and Remote Sensing Letters*, vol. 10, no. 3, pp. 543–547, 2013.
- [8] E. Aguilera, M. Nannini, and A. Reigber, "Wavelet-based compressed sensing for sar tomography of forested areas," *IEEE transactions on geoscience and remote sensing*, vol. 51, no. 12, pp. 5283–5295, 2013.
- [9] V. Cazcarra-Bes, M. Pardini, M. Tello, and K. Papathanassiou, "Comparison of tomographic sar reflectivity reconstruction algorithms for forest applications at l-band," *IEEE Transactions on Geoscience and Remote Sensing*, vol. 58, pp. 147–164, Jan 2020.
- [10] N. Levanon and E. Mozeson, *Radar Signals*. Wiley - IEEE, Wiley, 2004.
- [11] M. Nannini, R. Scheiber, and A. Moreira, "Estimation of the minimum number of tracks for sar tomography," *IEEE Transactions on Geoscience and Remote Sensing*, vol. 47, no. 2, pp. 531–543, 2009.
- [12] G. Fornaro, F. Serafino, and F. Soldovieri, "Three-dimensional focusing with multipass sar data," *IEEE Transactions on Geoscience and Remote Sensing*, vol. 41, no. 3, pp. 507–517, 2003.
- [13] M. Nannini, A. Reigber, and R. Scheiber, "A study on irregular baseline constellations in sar tomography," in *8th European Conference on Synthetic Aperture Radar*, pp. 1–4, VDE, 2010.